# Absence of local fluctuating dimers in superconducting Ir_{1−x}(Pt,Rh)_{x}Te_{2}

Runze Yu, S. Banerjee, H. C. Lei, Ryan Sinclair, M. Abeykoon, H. D. Zhou, C. Petrovic, Z. Guguchia, and E. S. Bozin

Phys. Rev. B **97**, 174515 — Published 18 May 2018

DOI: 10.1103/PhysRevB.97.174515

# Absence of Local Fluctuating Dimers in Superconducting $Ir_{1-x}(Pt,Rh)_xTe_2$

Runze Yu,[1,†] S. Banerjee,[2] H. C. Lei,[1,††] Ryan Sinclair,[3] M. Abeykoon,[4]
H. D. Zhou,[3] C. Petrovic,[1] Z. Guguchia,[1,5] and E. S. Bozin[1,*]
[1] *Condensed Matter Physics and Materials Science Department, Brookhaven National Laboratory, Upton, NY 11973, USA**
[2] *Department of Applied Physics and Applied Mathematics, Columbia University, New York, NY 10027, USA*
[3] *Department of Physics and Astronomy, University of Tennessee, Knoxville, Tennessee 37996, USA*
[4] *Photon Sciences Division, Brookhaven National Laboratory, Upton, NY 11973, USA and*
[5] *Department of Physics, Columbia University, New York, NY 10027, USA*

The compound $IrTe_2$ is known to exhibit a transition to a modulated state featuring Ir-Ir dimers, with large associated atomic displacements. Partial substitution of Pt or Rh for Ir destabilizes the modulated structure and induces superconductivity. It has been proposed that quantum critical dimer fluctuations might be associated with the superconductivity. Here we test for such local dimer correlations and demonstrate their absence. X-ray pair distribution function approach reveals that the local structure of $Ir_{0.95}Pt_{0.05}Te_2$ and $Ir_{0.8}Rh_{0.2}Te_2$ dichalcogenide superconductors with compositions just past the dimer/superconductor boundary is explained well by a dimer-free model down to 10 K, ruling out the possibility of there being nanoscale dimer fluctuations in this regime. This is inconsistent with the proposed quantum-critical-point-like interplay of the dimer state and superconductivity, and precludes scenarios for dimer fluctuations mediated superconducting pairing.

## I. INTRODUCTION

Unconventional superconductivity (SC) often emerges in the proximity of symmetry breaking electronic and magnetic orders upon their destabilization by chemical modifications, external pressure and fields, as seen in a diverse variety of quantum systems[1–3]. The pairing mechanism remains elusive[4], in part because the role of fluctuations of adjacent ordered states and their ubiquity are not fully established and understood[5–7]. Studying such fluctuations is quite challenging[8], one of the reasons being the lack of the long range coherence[9]. When broken symmetry states, for example electronic states involving $5d$ manifolds in $CuIr_2S_4$[10,11] and $IrTe_2$[12,13] where two $Ir^{4+}$ S=1/2 bind into spinless spatially ordered dimers, are coupled to the lattice, footprints of their fluctuations become evident in the local atomic structure and can be studied indirectly using a local structural probe[14,15] such as the atomic pair distribution function (PDF) analysis of powder diffraction data[16,17]. Here we use x-ray PDF to probe the existence or absence of $Ir^{4+}$-$Ir^{4+}$ dimer fluctuations in doped $IrTe_2$ superconductor, which yields information essential for bona fide considerations of dimer/SC entanglement in this system.

Trigonal metallic iridium ditelluride, $IrTe_2$, has garnered significant attention over the past several years following the discovery of bulk superconductivity ($T_c \sim$3 K) in its intercalated and substituted variants $IrTe_2$:Pd[18], $Ir_{1-x}Pt_xTe_2$[19], $Cu_xIrTe_2$[20], and $Ir_{1-x}Rh_xTe_2$[21]. Interestingly, the appearance of SC also follows the suppression of a long range ordered electronic state, in this case associated with charge disproportionation enabled $Ir^{4+}$-$Ir^{4+}$ dimerization[12,13] established in $IrTe_2$ at its symmetry lowering structural transition ($T_s \sim$250 K)[22]. This results in familiar domelike phase diagrams, akin to those of high temperature SCs and recently discovered $Cu_xTiSe_2$[23], 1T-$TaS_2$[24], 1T-$TiSe_2$[25], $T_d$-$MoTe_2$[26], $ZrTe_{3-x}Se_x$[27], and 2H-$TaSe_{2-x}S_x$[28] transition metal dichalcogenide superconductors, where destabilization of the charge density wave (CDW) order leads to SC. Importantly, in $Cu_xTiSe_2$ quantum criticality associated with fluctuations of CDW order has been considered in relation to SC pairing[29,30]. A perceived analogy with these systems prompted a hypothesis of quantum critical point (QCP) like interplay of SC and dimerization in $IrTe_2$ derivates[18], and speculations about dimer fluctuation mediated superconductivity[19,31].

The importance of the $IrTe_2$ lattice in facilitating the long range dimer order is well documented[32–34], with signatures of the dimer state found in a remarkable reduction of intradimer Ir-Ir (0.8 Å) and associated Te-Te (0.5 Å) distances[12], as illustrated in Fig. 1(a), (b). Despite this, and the importance of verifying the dimer fluctuations hypothesis, the utilization of experimental probes sensitive to presence/absence of local distortions has been surprisingly scarce. Existing reports based on extended x-ray absorption fine structure (EXAFS) spectroscopy focus on parent $IrTe_2$ under ambient[35] and high pressure[36] conditions. The ambient study argues for persistence of *local* Ir dimers in the high temperature regime where the structure is undistorted trigonal on average[35]. Whilst this, if true, could hint at the presence of fluctuating dimers also in the superconducting compositions, experimental validation is still lacking.

Here we employ the PDF approach on superconducting compositions of two different $Ir_{1-x}A_xTe_2$ families just across the dimer/SC boundary to explore for the first time the existence of local dimer fluctuations. Since the PDF probes instantaneous atomic arrangements[17], when structural dimers are present they should be observable in the local structure whether they are static or fluctuating. The PDF sensitivity to the presence of Ir-Ir dimers

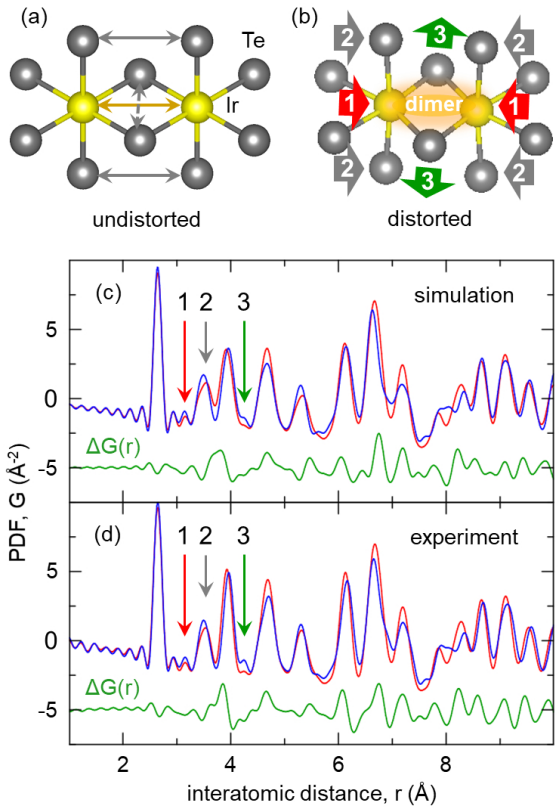


FIG. 1. (Color online) Sketch of the local atomic environments in $IrTe_2$ for the (a) undistorted high temperature structure (trigonal $P\bar{3}m1$), and (b) distorted low temperature structure (triclinic $P\bar{1}$) featuring Ir-Ir and Te-Te dimers. Dimerization results in dramatic distortions of associated interatomic distances relative to the high temperature structure, as indicated by block arrows and described in the text. Comparison of PDFs (c) calculated from trigonal (red line) and triclinic (blue line) models, and (d) measured at 275 K (red line) and at 220 K (blue line). Enumerated vertical arrows in (c) and (d) mark features associated with these distortions. $\Delta G(r)$ is the difference, offset for clarity.

irrespective of the character of their ordering has been demonstrated in $CuIr_2S_4$[10,37] and $Cu(Ir_{1-x}Cr_x)_2S_4$[38] spinels, where similar dimerization takes place on the Ir pyrochlore sublattice. When present, local dimers are clearly evident in the PDF of $IrTe_2$ due to the large change in the Ir-Ir and Te-Te interatomic distances associated with them. Here we provide conclusive evidence that the dimers are absent in $Ir_{0.95}Pt_{0.05}Te_2$ and $Ir_{0.8}Rh_{0.2}Te_2$ down to 10 K. This unambiguously rules out the popular hypothesis of quantum dimer fluctuations in this regime and that such fluctuations play a role in SC pairing. Moreover, PDF finds no evidence for dimer fluctuations in $IrTe_2$ at $T > T_s$, in stark contrast to previous EXAFS report[35].

## II. EXPERIMENTAL

Polycrystalline samples of $IrTe_2$, $Ir_{0.95}Pt_{0.05}Te_2$, and $Ir_{0.8}Rh_{0.2}Te_2$ were synthesized using standard solid-state protocols, and were found to be single phase based on x-ray powder diffraction[39,40]. Temperature dependent electrical transport and magnetization measurements on these samples were carried out on warming in *Quantum Design* PPMS-9 and MPMS-XL5. These data are shown in Fig. 2. There is a clear anomaly seen in the parent $IrTe_2$ associated with a simultaneous structural and electronic phase transition where long range dimer order is established. No such anomalies are seen in the data for $Ir_{0.95}Pt_{0.05}Te_2$ and $Ir_{0.8}Rh_{0.2}Te_2$ samples, implying the absence of a dimerization transition for these compositions. On the other hand, the low temperature resistivity and susceptibility data shown in the insets to the figure clearly demonstrate bulk superconductivity of these Pt and Rh substituted samples (vertical arrows indicate $T_c$).

Total scattering PDF experiments were performed at the 28-ID-2 beam line at the National Synchrotron Light Source II at Brookhaven National Laboratory, with 67.7 keV x-rays using the rapid acquisition mode with 60 s exposure for each dataset[41]. The setup utilized *Perkin-Elmer* area detector and *Cryoindustries of America* cryostat for data collection between 10 K and 300 K on warming. The raw 2D diffraction data were integrated and converted to intensity versus $Q$ using the software FIT2D[42], where $Q$ is the magnitude of the scattering vector. Data reduction to measured total scattering struc-

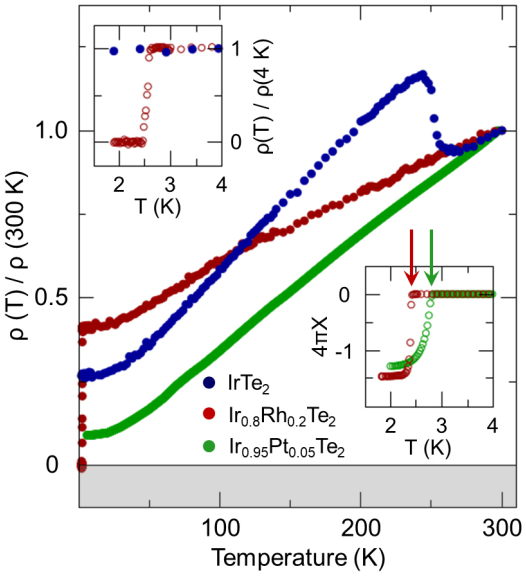


FIG. 2. (Color online) Electrical resistivity of $IrTe_2$, $Ir_{0.95}Pt_{0.05}Te_2$, and $Ir_{0.8}Rh_{0.2}Te_2$ samples, normalized to their 300 K values. Insets: (upper left corner) low temperature resistivity, and (lower right corner) low temperature susceptibility collected in the zero field cooling mode.

ture functions, $F(Q)$, and their successive Sine Fourier transform up to a momentum transfer of $Q_{max} = 25$ Å$^{-1}$ to obtain experimental PDFs, $G(r)$, were carried out using the PDFGETX3[43] program. Models with P$\bar{3}$m1 and P$\bar{1}$ symmetry were used to describe nondimerized (Fig. 1(a)) and dimerized (Fig. 1(b)) structures, respectively, using the PDFGUI suite[44].

## III. RESULTS

We begin by establishing qualitatively the sensitivity of our PDF data to the presence of dimers and concomitant structural distortions in $IrTe_2$. In the high temperature phase above $T_s$ all Ir atoms are in identical $Te_6$ octahedral environments displaying an edge-shared topology, Fig. 1(a), constituting trigonal symmetry average structure[45]. In the low temperature phase just below $T_s$, where the dimer patterns with a stripe morphology corresponding to $\mathbf{q}_0 = 1/5(1, 0, 1)$ ordering are established[18,32], Ir atoms subject to dimerization sit in distorted $Te_6$ octahedral environments, Fig. 1(b), and the average symmetry lowers to triclinic[12]. Pairs of dimerization-affected $IrTe_6$ octahedra exhibit dramatic structural rearrangements: Ir-Ir and Te-Te dimer distances reduce by 0.8 Å and 0.5 Å respectively, while the lateral Te-Te distance (common edge) elongates by 0.3 Å[12]. The distortions are depicted by enumerated block arrows in Fig. 1(b). Importantly, only $\sim 6$ % of all nearest neighbor Ir-Ir distances on triangular Ir planes of $IrTe_2$ dimerize, in contrast to $CuIr_2S_4$ where the fraction of dimerized Ir contacts is about 5 times larger[10].

We simulated PDF patterns for the average crystal structures for $T > T_s$ (trigonal) and $T < T_s$ (triclinic) using parameters from single crystal x-ray diffraction[12]. These are shown in Fig. 1(c) as red and blue profiles, respectively, with their difference plotted underneath. Changes in the interatomic distance distribution arising from dimerization as seen by PDF are marked by enumerated vertical arrows. Examination of the high and low temperature profiles reveals a redistribution of intensity in PDF peaks centered around 3.5 Å (Te-Te) and 3.9 Å (lattice repeat distance), whereas new peaks appear at around 3.1 Å (Ir-Ir dimer), 3.4 Å (Te-Te dimer), and 4.2 Å (common Te-Te edge). It is evident that the Ir-Ir dimer signal at 3.1 Å is rather weak, as compared to that observed in $CuIr_2S_4$ spinel[37], and is barely visible above the parapet of termination ripples caused by the finite range of the Fourier transform. This comes about due to different dimer densities in the two materials. However, this analysis shows that, despite this relatively weaker signal, the PDF is still sensitive to the presence or absence of local dimers.

Experimental PDFs of $IrTe_2$ for temperatures straddling $T_s$ are compared in Fig. 1(d), where the 275 K (red profile, $T > T_s$) and the 220 K (blue profile, $T < T_s$) data and their difference are displayed. A qualitative assessment readily demonstrates that all dimerization features described above and highlighted in the calculated PDFs, which contain the impact of the dimers, are well reproduced in the experimental PDF data. This clearly establishes the PDF sensitivity to dimer structural signatures and their detectability in our data. Comparisons in Figs. 1 (c) and (d) also indicate that the dimers *disappear* in the local structure above $T_s$, as is further confirmed by explicit modeling that we discuss later. Notably, proposed order-disorder scenario for the dimerization transition[35] is at odds with this observation. The first-order nature of the transition[22,32] also argues against the persistence of local fluctuating dimers above $T_s$.

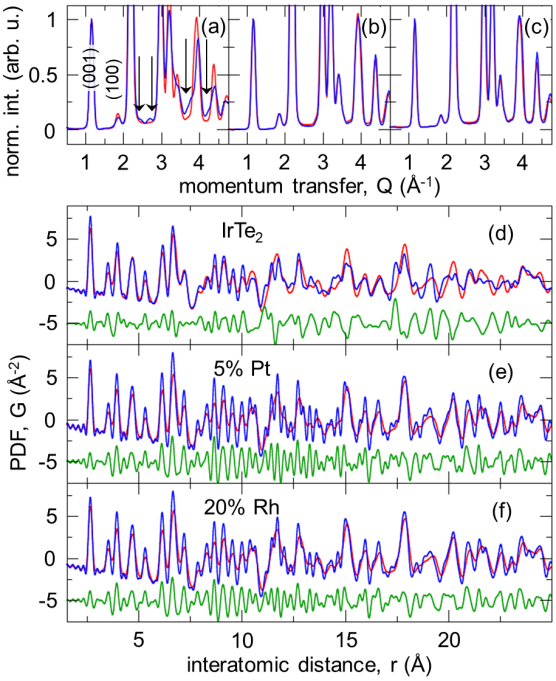


FIG. 3. (Color online) Azimuthally integrated 2D diffraction patterns of $Ir_{1-x}(Pt,Rh)_xTe_2$ for 300 K (red line) and 10 K (blue line) over a narrow range of momentum transfer, $Q$, for (a) x=0, (b) x=0.05 Pt, and (c) x=0.2 Rh. All patterns are normalized by the intensity of (001) reflection (P$\bar{3}$m1 indexing). Vertical arrows in (a) indicate superlattice reflections observed in 10 K data. Corresponding PDFs are compared in (d), (e), and (f), respectively, with differences shown underneath and offset for clarity.

Samples with SC compositions display qualitatively different behavior on all lengthscales accessible by our measurements. When the average $IrTe_2$ symmetry is lowered and the long range dimer order is established, superlattice reflections appear in the integrated diffraction patterns, as seen in Fig. 3(a) where 10 K and 300 K are compared. In contrast, no such features are observed in $Ir_{0.95}Pt_{0.05}Te_2$ (Fig. 3(b)) and $Ir_{0.8}Rh_{0.2}Te_2$ (Fig. 3(c)) data at any temperature, consistent with the average symmetry remaining trigonal down to 10 K and no long range dimer order, as expected from the monotonic temperature variation of susceptibility and electrical resistivity[19,21]. Importantly, the dimers are also not observed at

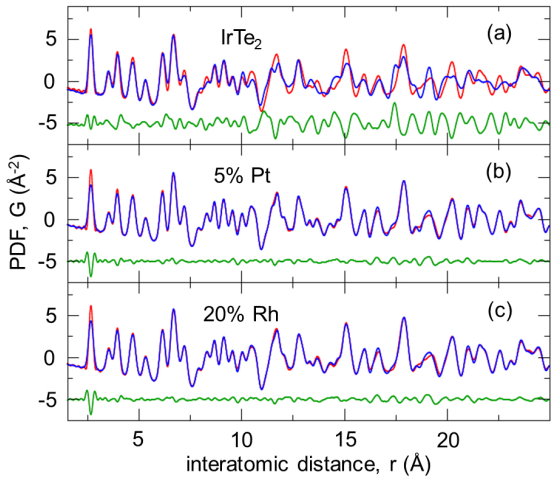


FIG. 4. (Color online) A comparison of the 10 K (blue) and 300 K (red) PDF data for (a) $IrTe_2$, (b) $Ir_{0.95}Pt_{0.05}Te_2$, and (c) $Ir_{0.8}Rh_{0.2}Te_2$, where the 10 K data were adjusted in a simple optimization procedure described in the text. Differences are plotted underneath and offset for clarity.

low temperature on intermediate and short lengthscales probed by the PDF. When symmetry lowering occurs, this causes redistribution of PDF intensities and overall broadening of the PDF patterns due to the appearance of new interatomic distances. Conversely, temperature lowering sharpens the PDF features as a consequence of decreasing the amplitudes of thermal vibrations[17]. Both effects are present in $IrTe_2$ PDFs, Fig. 3(d), where the 300 K profile is observably sharper than that of 10 K at intermediate $r$, and their difference reveals a change corresponding to a superposition of these two opposite effects. Figs. 3 (e) and (f) show 300 K and 10 K data for superconducting samples. Whilst there are also dramatic changes evidenced in the respective difference curves, this is qualitatively different from what is seen in $IrTe_2$.

## IV. DISCUSSION

It can be shown through a semiempirical scaling procedure that high and low temperature PDFs of doped samples can be successfully morphed into each other, whereas such a procedure fails in the case of $IrTe_2$. Figure 4 summarizes the comparisons of qualitative features of the 10 K and 300 K PDF data for the three samples studied. For the comparisons, the low temperature PDF profiles were subjected to a simple semiempirical protocol, dubbed morphing and described below. The morphing analysis indicates that, while symmetry breaking is required to explain the differences observed in the $IrTe_2$ data, the differences observed in the $Ir_{0.95}Pt_{0.05}Te_2$ and $Ir_{0.8}Rh_{0.2}Te_2$ data are likely due to mundane thermal effects only.

The morphing comparison procedure allows for an assessment of similarities of two sets of PDF data to be carried out without an assumption of any specific structure model. This allows, at least in principle, a differentiation between symmetry breaking effects and trivial lattice expansion effects as sources of the observed differences, such as those shown in Fig. 3(d)-(f). In the morphing protocol one of the two experimental PDFs is selected as a reference, and is not being altered in any way (300 K data here). The other of the two profiles to be compared (10 K data in this case) is subjected to the morphing procedure. This is parametrized by three variables - horizontal and vertical linear scale factors, which stretch the $r$ and $G$ axes respectively, and a smear parameter that convolutes the subjected PDF with a Gaussian of fixed width. A least squares optimization protocol utilizing these three variables is then carried out until the best possible match between the morph and the reference PDFs is achieved. This is quantified by minimizing the weighted residual, $r_w$, of the PDF difference and by maximizing the Pearson correlation coefficient, $P$. In the case of ideal morphing $r_w$ would be 0, whereas $P$ would take a value of 1, reflecting perfect agreement between the morph and the reference PDF and a 100% positive correlation between the two profiles whose similarity is being evaluated. Formal mathematical treatment and more involved details of this protocol will be reported elsewhere. When the difference between the two measured PDFs originates from trivial lattice effects, such as thermal expansion, morphing results in a low value of $r_w$ and the Pearson correlation coefficient close to 1. Conversely, when the difference originates from more complex effects, such as symmetry breaking, morphing results in suboptimal values of $r_w$ and $P$.

To benchmark the comparison of our PDF data at 10 K and 300 K when no morphing is applied (Fig. 3 (d)-(f)), we calculated ($r_w$, $P$) pairs for all three samples studied. This benchmarking yields (0.52, 0.86), (0.65, 0.89), and (0.56, 0.91) for $IrTe_2$, $Ir_{0.95}Pt_{0.05}Te_2$, and $Ir_{0.8}Rh_{0.2}Te_2$, respectively. On the other hand, the fully converged morphing yields (0.46, 0.89), (0.14, 0.99), and (0.15, 0.99), for $IrTe_2$, $Ir_{0.95}Pt_{0.05}Te_2$, and $Ir_{0.8}Rh_{0.2}Te_2$, respectively. Comparison of the observed $r_w$ and $P$ values with the benchmark references reveals that these parameters improve considerably by morphing in the case of $Ir_{0.95}Pt_{0.05}Te_2$ and $Ir_{0.8}Rh_{0.2}Te_2$, but do not improve much at all for the $IrTe_2$ parent. Corresponding difference curves shown in Figure 4 reflect this as well. This analysis suggests that the difference in PDFs for SC samples is likely caused only by simple lattice effects without any symmetry breaking. This conclusion is further supported by the fact that the protocol successfully singles out symmetry breaking in $IrTe_2$, as is expected when comparing the two datasets straddling the structural transition.

Although the morphing of the data for the SC samples is reasonably good, it is observably non-ideal, as evident from a careful inspection of the difference curves shown in Fig. 4 (b) and (c). While the discrepancies could indicate underlying symmetry breaking, the more

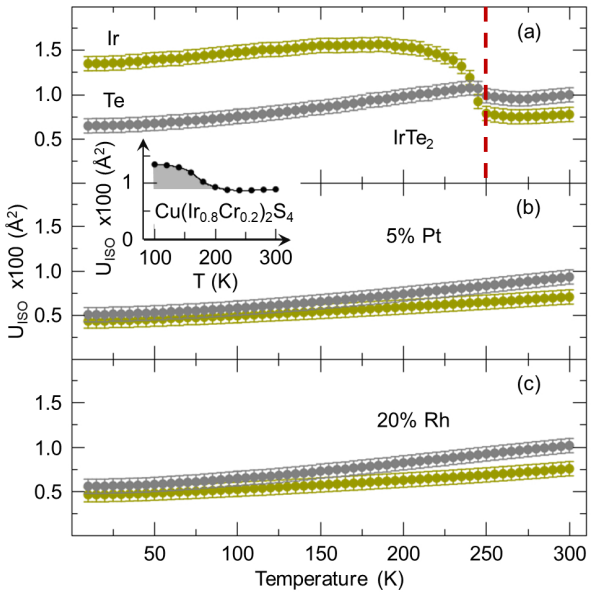


FIG. 5. (Color online) Temperature dependence of the isotropic ADPs of Ir (olive symbols) and Te (gray symbols) in $Ir_{1-x}(Pt,Rh)_xTe_2$ obtained from P$\bar{3}$m1 model fits to (a) x=0, (b) x=0.05 Pt, and (c) x=0.2 Rh sample data over the 10 K–300 K temperature range. Inset: detection of onset of dimer fluctuations from temperature dependent Ir-ADP in 20% Cr-doped $CuIr_2S_4$, where Ir-Ir dimerization sets in below 200 K on a nanometer length-scale *only*, while the long range dimer order is absent at all temperatures[38]. Such behavior is *not* observed in (b) and (c) for superconducting $Ir_{1-x}(Pt,Rh)_xTe_2$.

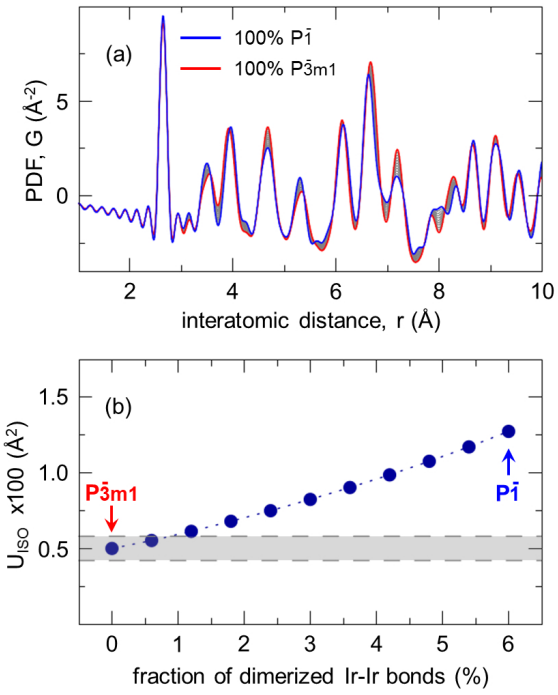


FIG. 6. (Color online) Quantification of PDF sensitivity to the presence of dimers. (a) Simulated PDFs of $IrTe_2$ comprised of mixtures of dimer (P$\bar{1}$) and non-dimer (P$\bar{3}$m1) phases, with the mixing ratio incrementing by 0.1. The different solid profiles correspond to dimer fractions ranging from 6% of dimerized Ir-Ir nearest neighbors (as observed in P$\bar{1}$ phase, blue) to no dimers (as is the case for P$\bar{3}$m1, red). PDFs for the intermediates are shown in gray. (b) Isotropic ADP of Ir obtained by fitting dimer-free P$\bar{3}$m1 model to the simulated PDFs in (a) as a function of absolute fraction of dimerized Ir-Ir bonds. The gray shaded region represents typical uncertainty on $2\sigma$ level in determining this parameter from the experimental PDFs using the same P$\bar{3}$m1 model.

likely reason behind this lies in the oversimplifications upon which the morphing algorithm is based. The three parameters allowing for scaling, stretching, and smearing of the subjected PDF profile effectively mimic only spherically uniform and isotropic thermal effects, whereas in a real material thermal expansion and thermal vibrations have more complex impact on the PDF profile. Notably, the largest discrepancies observed in Fig. 4 (b) and (c) are confined to a narrow $r$-range just underneath the first PDF peak around 2.5 Å. This region is known to be affected by the correlated motion of the nearest neighbors[17], an effect not accounted for in the morphing procedure. Despite these shortcomings the morphing analysis rather intuitively suggests that the changes in the SC samples are likely caused solely by thermal effects, without symmetry lowering, whereas the actual symmetry breaking is needed to explain the changes in the parent system.

To further search for the evidence that would indicate local dimerization in the SC samples we assess the temperature evolution of structural modeling parameters that are sensitive to the presence of disorder[38]. Undistorted trigonal P$\bar{3}$m1 model was refined in the $r$-space against the PDF data in 10 K–300 K range for all three samples studied, and the obtained atomic displacement parameters (ADPs) monitored, Fig. 5. While in $IrTe_2$ both ADPs of Ir and Te initially drop linearly with temperature, Fig. 5(a), they exhibit an abrupt jump at the onset of the dimerization transition, denoted by vertical dashed red line in the figure. This nominally implies "disorder", but actually reflects the inadequacy of the trigonal model to explain the symmetry breaking and underlying dimerization encoded in the data. In contrast, no such jumps are observed for $Ir_{0.95}Pt_{0.05}Te_2$ (Fig. 5(b)) and $Ir_{0.8}Rh_{0.2}Te_2$ (Fig. 5(c)) in the entire temperature range studied. It is important to realize that jumps in ADPs are not only observed across long range symmetry breaking transitions, but also in cases when there is only a local structure change in the absence of any macroscopic transitions. The inset in Fig. 5 exemplifies such a situation seen in 20% Cr-doped $CuIr_2S_4$, where *local* Ir-Ir dimerization sets in just below 200 K, in the absence of long range dimer order at any temperature in that system[38]. This demonstrates that there is neither average nor local symmetry lowering in $Ir_{0.95}Pt_{0.05}Te_2$ and $Ir_{0.8}Rh_{0.2}Te_2$ down to 10 K.

To quantitatively estimate the PDF sensitivity to the presence of dimers in $IrTe_2$ as seen through the ADP pa-

rameters, we carried out a test on a set of simulated data as follows. To mimic the dimer density variation between 0% and 6% (full dimer density observed in the ordered phase with $\mathbf{q}_0 = 1/5(1, 0, 1)$), we used a two phase model comprising of the dimerized ($P\bar{1}$) and dimer-free ($P\bar{3}m1$) components. Corresponding PDFs were simulated for a range of mixing fractions (Fig. 6 (a)). These simulated PDF data were subsequently fit by the same dimer-free $P\bar{3}m1$ model as used for the experimental data to obtain ADPs that are shown in Fig. 5. Values of Ir ADP obtained from fitting such synthetic data are then plotted against the fraction of dimerized Ir-Ir bonds (known from simulations), and the plot is overlayed with the uncertainty window centered around the ADP value corresponding to zero dimer density, as shown in Fig. 6 (b). The width of the uncertainty window (gray shaded area in the figure) corresponds to a typical estimated standard deviation on $2\sigma$ level obtained from the fits to the experimental data (the error bars in Fig. 5). The sensitivity is defined as the value of the dimerized Ir-Ir fraction for which the ADP value of Ir sinks into the gray shaded region. The sensitivity floor is about 0.5% of dimerized Ir-Ir bonds (99.5% of Ir-Ir bonds are not dimerized). This corresponds to the dimer density that is *order of magnitude* smaller than that observed in the $\mathbf{q}_0 = 1/5(1, 0, 1)$ ordered phase. This establishes the dimer detectability floor from our measurements in $IrTe_2$ from Ir-ADPs to be below ∼0.5%

It is noteworthy that the values of ADP parameters for both Ir and Te at 300 K obtained for $Ir_{0.95}Pt_{0.05}Te_2$ and $Ir_{0.8}Rh_{0.2}Te_2$ are comparable to those observed in $IrTe_2$ (Fig. 5). This indicates that any quenched disorder introduced by substituting Pt and Rh for Ir is immesurably small, as one may also expect from their rather similar ionic radii[46]. Substantial disorder induced strain is known to stabilize the local Ir dimer state in related $Cu(Ir_{1-x}Cr_x)_2S_4$ dimer system, and is in fact believed to be behind the appearance of local dimers at low temperature for Cr concentrations above 15% in the absence of the long range dimer order (see inset to Fig. 5)[38]. On the other hand, it has been established recently that external pressure stabilizes the dimer state in $Ir_{1-x}Pt_xTe_2$[34]. It is therefore reasonable to expect that any substitution related strains, if present, would likely enhance local dimerization in the $IrTe_2$ system, rather than suppress it. Taken together, this implies that substitutional disorder is not responsible for the lack of observable signal that would indicate dimerization in SC compositions of $IrTe_2$.

Lastly, we consider the actual fits of the trigonal structure model to various PDF data over the 10 Å range, shown in Fig. 7 as solid red lines and open blue symbols, respectively. This undistorted dimer-free model explains the $IrTe_2$ 300 K data exceptionally well, Fig. 7(a), as evident from the flat difference curve and a low fit residual value of $r_w$ ∼4%. The same model fails to explain the $IrTe_2$ data at 10 K ($r_w$ ∼15%), in Fig. 7(b), as expected, given that at that temperature long range dimer order is well established and that the attempted dimer-free model

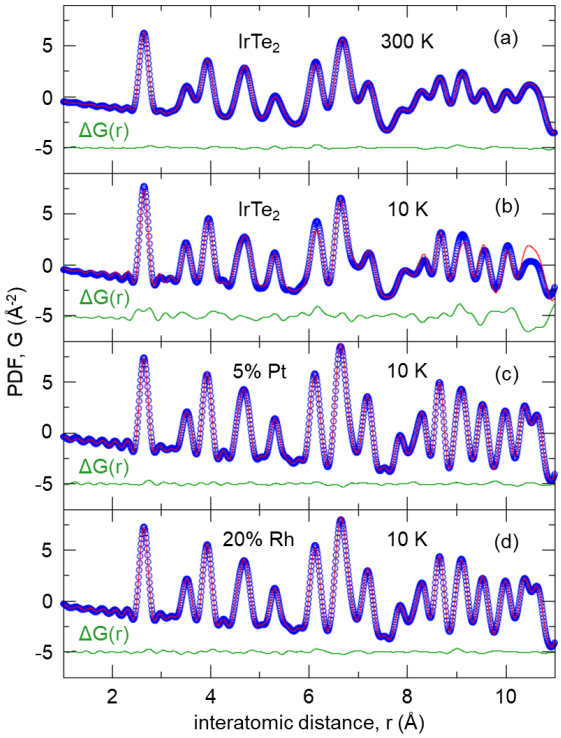


FIG. 7. (Color online) Fits of trigonal structure model (solid red lines) to experimental PDF data (open blue symbols) of $IrTe_2$ sample at (a) 300 K and (b) 10 K, 5 % Pt substituted sample at 10 K (c), and 20 % Rh substituted sample at 10 K (d). The difference between the data and the model, $\Delta G(r)$, plotted below, is offset for clarity. See text for details.

is strictly inadequate. Importantly, this failed fit charts substantial misfits in the difference curve that would reveal the presence of dimers in the data when they are confronted with a dimer-free model. Figs. 7(c) and (d) show the results of such a fitting attempt carried out on 10 K $Ir_{0.95}Pt_{0.05}Te_2$ and $Ir_{0.8}Rh_{0.2}Te_2$ data, respectively. Not only do the corresponding difference curves not display the features observed in Fig. 7(b), but the fits of the trigonal model in fact agree rather well with the data ($r_w$ ∼5%). The local structure at 10 K for these compositions is well explained by a dimer-free model. This quantitative analysis validates the aforementioned qualitative conclusions about the absence of dimer fluctuations in the high temperature phase of the parent system as well as at 10 K in superconducting compositions just past the dimer/SC boundary. The transition in $IrTe_2$ is argued to originate from a uniform lattice deformation combined with charge ordering and subsequent Ir dimerization[33], with the structural transition as a trigger[34]. Putative quantum critical fluctuations will thus inevitably appear in the structural channel.

Further, importan insights can also be gained from the analysis of the diamagnetic response to dimerization in magnetic susceptibility in $Ir_{1-x}Pt_xTe_2$ and $Ir_{1-x}Rh_xTe_2$. Namely, dimerization transition in $IrTe_2$ is accompanied by anomalies in both resistivity (jump) and magnetic

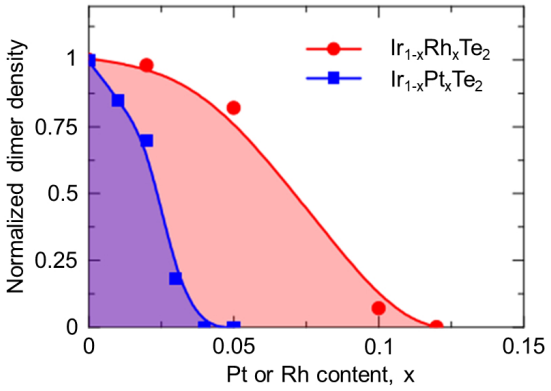


FIG. 8. (Color online) Normalized dimer density as a function of Pt and Rh content in $IrTe_2$ estimated from published magnetic susceptibility measurements[19,21].

susceptibility (dip). Superconductivity is invoked upon suppression of the transition by chemical substitution in $Ir_{1-x}Pt_xTe_2$[19] and $Ir_{1-x}Rh_xTe_2$[21]. In both systems substitution causes the transition temperature to decrease with increasing the substitute content. In addition to this, the dip in susceptibility, corresponding to the dimerization related diamagnetic reduction of the total magnetic susceptibility, becomes smaller and eventually disappears in the superconducting range of compositions past the dimer/SC boundary[19,21].

It can be inferred from a combination of magnetic susceptibility, Ir $4f$ core-level photoemission spectroscopy (PES), and scanning tunneling microscopy (STM) measurements that this drop is proportional to the static dimer density[47]. Systematic study of Ko *et al.* reveals two dimerization related phase transitions on cooling in high quality single crystal of $IrTe_2$, one at ∼280 K associated with $\mathbf{q}_{1/5} = 1/5(1, 0, 1)$ order, followed by another one at ∼180 K associated with $\mathbf{q}_{1/8} = 1/8(1, 0, 1)$ order. The PES measurements reveal that the $Ir^{4+}$:$Ir^{3+}$ ratio increases at the lower transition temperature. At the same time, according to the assessment of the STM images, the dimer density is found to increase on going from $\mathbf{q}_{1/5}$ to $\mathbf{q}_{1/8}$ phase. Importantly, magnetic susceptibility dips twice, first at ∼280 K, and then again at ∼180 K. Taken together, this implies that the size of the dip is proportional to the static dimer density.

Here we estimate the static dimer density for $Ir_{1-x}Pt_xTe_2$ and $Ir_{1-x}Rh_xTe_2$ as a function of Pt and Rh content from the size of the susceptibility dip taken from the reported data collected on warming[19,21]. This is shown in Fig. 8, where the density is further normalized to the value for $IrTe_2$. This estimate clearly reveals that the static dimer density decreases gradually with chemical substitution, and vanishes for SC compositions.

The PDF findings presented here rule out the presence of dimers, both static *and dynamic*, and impose the upper limit of 0.5% on the number of Ir pairs that could be dimerized in the SC range of compositions. Further systematic investigations utilizing techniques sensitive to fluctuations and local structure acrost the phase diagrams of $Ir_{1-x}Pt_xTe_2$ and $Ir_{1-x}Rh_xTe_2$ would be highly desirable and to provide further insights on the interplay of these quantum orders, particularly in the vicinity of the dimer/SC boundary.

## V. CONCLUSIONS

In summary, by using state of the art x-ray total scattering based PDF approach we establish the first direct evidence for the absence of local dimer fluctuations in the phase diagrams of $Ir_{1-x}Pt_xTe_2$ and $Ir_{1-x}Rh_xTe_2$ beyond the dimer/superconductor phase boundary. The dimer fluctuations are also absent in the parent $IrTe_2$ in the temperature regime above the structural phase transition. These results imply that dimer fluctuations are not a relevant part of the phase diagram of $IrTe_2$ based systems and thus their role in the superconducting pairing is implausible. The results provide important new constraints for theoretical considerations of the complex interplay between superconductivity and other electronic orders in this class of materials.

## ACKNOWLEDGMENTS

Work at Brookhaven National Laboratory was supported by US DOE, Office of Science, Office of Basic Energy Sciences (DOE-BES) under contract DE-SC00112704. R. Sinclair and H. D. Zhou acknowledge support from NSF-DMR-1350002. We are grateful to John Tranquada, Simon Billinge, Ian Robinson, Igor Zaliznyak, Alexandros Lappas, and Alexei Tsvelik for fruitful discussions and critical comments.

* bozin@bnl.gov
†Present address: Institute of Physics, Chinese Academy of Science, Beijing, 100190, Peoples Republic of China
†† Present address: Department of Physics, Renmin University, Beijing 100872, Peoples Republic of China

[1] D. N. Basov and A. V. Chubukov, Nature Phys. **7**, 272 (2011).
[2] G. Saito and Y. Yoshida, Chem. Rec. **11**, 124 (2011).
[3] L. Jiao, Y. Chen, Y. Kohama, D. Graf, E. Bauer, J. Singleton, J. Zhu, Z. Weng, G. Pang, T. Shang, J. Zhang, H. O. Lee, T. Park, M. Jaime, J. D. Thompson, F. Steglich, Q. Si, and H. Q. Yuan, Proc. Natl. Acad. Sci. USA **112**, 673 (2015).
[4] M. R. Norman, Science **332**, 196 (2011).
[5] P. A. Lee, N. Nagaosa, and X. Wen, Rev. Mod. Phys. **78**, 17 (2006).

[6] J. Chang, E. Blackburn, A. T. Holmes, N. B. Christensen, J. Larsen, J. Mesot, R. Liang, D. A. Bonn, W. N. Hardy, A. Watenphul, M. v. Zimmermann, E. M. Forgan, and S. M. Hayden, Nature Phys. **8**, 871 (2010).

[7] R. Comin, A. Frano, M. Yee, Y. Yoshida, H. Eisaki, E. Schierle, E. Weschke, R. Sutarto, F. He, A. Soumyanarayanan, Y. He, M. Le Tacon, I. S. Elfimov, J. E. Hoffman, G. A. Sawatzky, B. Keimer, and A. Damascelli, Science **343**, 390 (2014).

[8] S. A. Kivelson, I. P. Bindloss, E. Fradkin, V. Oganesyan, J. M. Tranquada, A. Kapitulnik, and C. Howald, Rev. Mod. Phys. **75**, 1201 (2003).

[9] S. J. L. Billinge and I. Levin, Science **316**, 561 (2007).

[10] P. G. Radaelli, Y. Horibe, M. J. Gutmann, H. Ishibashi, C. H. Chen, R. M. Ibberson, Y. Koyama, Y. S. Hor, V. Kiryukhin, and S.-W. Cheong, Nature **416**, 155 (2002).

[11] D. I. Khomskii and T. Mizokawa, Phys. Rev. Lett. **94**, 156402 (2005).

[12] G. L. Pascut, K. Haule, M. J. Gutmann, S. A. Barnett, A. Bombardi, S. Artyukhin, T. Birol, D. Vanderbilt, J. J. Yang, S.-W. Cheong, and V. Kiryukhin, Phys. Rev. Lett. **112**, 086402 (2014).

[13] T. Toriyama, M. Kobori, T. Konishi, Y. Ohta, K. Sugimoto, J. Kim, A. Fujiwara, S. Pyon, K. Kudo, and M. Nohara, J. Phys. Soc. Jpn **83**, 033701 (2014).

[14] J. Lee, K. Fujita, K. McElroy, J. A. Slezak, M. Wang, Y. Aiura, H. Bando, M. Ishikado, T. Masui, J. X. Zhu, A. V. Balatsky, H. Eisaki, S. Uchida, and J. C. Davis, Nature **442**, 546 (2006).

[15] E. S. Božin, M. Schmidt, A. J. DeConinck, G. Paglia, J. F. Mitchell, T. Chatterji, P. G. Radaelli, T. Proffen, and S. J. L. Billinge, Phys. Rev. Lett. **98**, 137203 (2007).

[16] S. J. L. Billinge, J. Solid State Chem. **181**, 1695 (2008).

[17] T. Egami and S. J. L. Billinge, *Underneath the Bragg peaks: structural analysis of complex materials* (Elsevier, Amsterdam, 2012), 2nd ed.

[18] J. J. Yang, Y. J. Choi, Y. S. Oh, A. Hogan, Y. Horibe, K. Kim, B. I. Min, and S.-W. Cheong, Phys. Rev. Lett. **108**, 116402 (2012).

[19] S. Pyon, K. Kudo, and M. Nohara, J. Phys. Soc. Jpn **81**, 053701 (2012).

[20] M. Kamitani, M. S. Bahramy, R. Arita, S. Seki, T. Arima, Y. Tokura, and S. Ishiwata, Phys. Rev. B **87**, 180501 (2013).

[21] K. Kudo, M. Kobayashi, S. Pyon, and M. Nohara, J. Phys. Soc. Jpn **82**, 085001 (2013).

[22] N. Matsumoto, K. Taniguchi, R. Endoh, H. Takano, and S. Nagata, J. Low Temp. Phys. **117**, 1129 (1999).

[23] E. Morosan, H. W. Zandbergen, B. S. Dennis, J. W. G. Bos, Y. Onose, T. Klimczuk, A. P. Ramirez, N. P. Ong, and R. J. Cava, Nature Phys. **2**, 544 (2006).

[24] B. Sipos, A. F. Kusmartseva, A. Akrap, H. Berger, L. Forro, and E. Tutis, Nature Mater. **7**, 960 (2008).

[25] A. F. Kusmartseva, B. Sipos, H. Berger, L. Forro, and E. Tutis, Phys. Rev. Lett. **103**, 236401 (2009).

[26] Z. Guguchia, F. von Rohr, Z. Shermadini, A. T. Lee, S. Banerjee, A. R. Wieteska, C. A. Marianetti, B. A. Frandsen, H. Luetkens, Z. Gong, S. C. Cheung, C. Baines, A. Shengelaya, G. Taniashvili, A. N. Pasupathy, E. Morenzoni, S. J. L. Billinge, A. Amato, R. J. Cava, R. Khasanov, and Y. J. Uemura, Nat. Commun. **8**, 1082 (2017).

[27] X. Zhu, W. Ning, L. Li, L. Ling, R. Zhang, J. Zhang, K. Wang, Y. Liu, L. Pi, Y. Ma, H. Du, M. Tian, Y. Sun, C. Petrovic, and Y. Zhang, Sci. Rep. **6**, 26974 (2016).

[28] L. Li, X. Deng, Z. Wang, Y. Liu, M. Abeykoon, E. Dooryhee, A. Tomic, Y. Huang, J. B. Warren, E. S. Bozin, S. J. L. Billinge, Y. Sun, Y. Zhu, G. Kotliar, and C. Petrovic, npj Quantum Materials **2**, 11 (2017).

[29] H. Barath, M. Kim, J. F. Karpus, S. L. Cooper, P. Abbamonte, E. Fradkin, E. Morosan, and R. J. Cava, Phys. Rev. Lett. **100**, 106402 (2008).

[30] A. H. Castro Neto, Phys. Rev. Lett. **86**, 4382 (2001).

[31] J. Dai, K. Haule, J. J. Yang, Y. S. Oh, S.-W. Cheong, and W. Wu, Phys. Rev. B **90**, 235121 (2014).

[32] Y. S. Oh, J. J. Yang, Y. Horibe, and S.-W. Cheong, Phys. Rev. Lett. **110**, 127209 (2013).

[33] K. Kim, S. Kim, K.-T. Ko, H. Lee, J.-H. Park, J. J. Yang, S.-W. Cheong, and B. I. Min, Phys. Rev. Lett. **114**, 136401 (2015).

[34] O. Ivashko, L. Yang, D. Destraz, E. Martino, Y. Chen, C. Y. Guo, H. Q. Yuan, A. Pisoni, P. Matus, S. Pyon, K. Kudo, M. Nohara, L. Forró, H. M. Rønnow, M. Hücker, M. v. Zimmermann, and J. Chang, Sci. Rep. **7**, 17157 (2017).

[35] B. Joseph, M. Bendele, L. Simonelli, L. Maugeri, S. Pyon, K. Kudo, M. Nohara, T. Mizokawa, and N. L. Saini, Phys. Rev. B **88**, 224109 (2013).

[36] E. Paris, B. Joseph, A. Iadecola, C. Marini, H. Ishii, K. Kudo, S. Pascarelli, M. Nohara, T. Mizokawa, and N. L. Saini, Phys. Rev. B **93**, 134109 (2016).

[37] E. S. Božin, A. S. Masadeh, Y. S. Hor, J. F. Mitchell, and S. J. L. Billinge, Phys. Rev. Lett. **106**, 045501 (2011).

[38] E. S. Božin, K. R. Knox, P. Juhás, Y. S. Hor, J. F. Mitchell, and S. J. L. Billinge, Sci. Rep. **4**, 4081 (2014).

[39] H. Cao, B. C. Chakoumakos, X. Chen, J. Yan, M. A. McGuire, H. Yang, R. Custelcean, H. D. Zhou, D. J. Singh, and D. Mandrus, Phys. Rev. B **88**, 115122 (2013).

[40] N. Lazarevic, E. S. Bozin, M. Scepanovic, M. Opacic, H. Lei, C. Petrovic, and Z. V. Popovic, Phys. Rev. B **89**, 224301 (2014).

[41] P. J. Chupas, X. Qiu, J. C. Hanson, P. L. Lee, C. P. Grey, and S. J. L. Billinge, J. Appl. Crystallogr. **36**, 1342 (2003).

[42] A. P. Hammersley, S. O. Svenson, M. Hanfland, and D. Hauserman, High Pressure Res. **14**, 235 (1996).

[43] P. Juhás, T. Davis, C. L. Farrow, and S. J. L. Billinge, J. Appl. Crystallogr. **46**, 560 (2013).

[44] C. L. Farrow, P. Juhás, J. Liu, D. Bryndin, E. S. Božin, J. Bloch, T. Proffen, and S. J. L. Billinge, J. Phys: Condens. Mat. **19**, 335219 (2007).

[45] E. F. Hockings and J. G. White, J. Phys. Chem. **64**, 1042 (1960).

[46] R. D. Shannon, Acta Crystallogr. A **32**, 751 (1976).

[47] K.-T. Ko, H.-H. Lee, D.-H. Kim, J.-J. Yang, S.-W. Cheong, M. J. Eom, J. S. Kim, R. Gammag, K.-S. Kim, H.-S. Kim, T.-H. Kim, H.-W. Yeom, T.-Y. Koo, H.-D. Kim, and J.-H. Park, Nature Commun. **6**, 7342 (2015).